Journal of Welding Technology
P-ISSN: 2716-1471 | E-ISSN: 2716-0475
http://e-jurnal.pnl.ac.id/Welding_Technology

The Influence of Prandtl Number on Flow Characteristics of the Fume from GMAW Welding

Luthfi
Department of Mechanical Engineering, State Polytechnic of Lhokseumawe,
Lhokseumawe 24301, Indonesia
Corresponding author: luthfi@pnl.ac.id

Article Processing Dates:
Received 2023-06-20
Accepted 2023-10-30
Available online 2023-12-30

Keywords:
GMAW
Fume
Health and safety
Prandtl number
CFD simulation

Abstract

GMAW has become one of the most popular welding methods due to its high productivity in the manufacturing industry. However, there has been agrowing concern about the health effects of the fume produced by this welding method, as it may flow into the breathing zone of the welding operator.In this study, the impact of the Pr number on the behavior of the fume flow produced by GMAW was studied numerically using Computational Fluid Dynamics (CFD) simulation. Navier-Stokes and energy equations in two-dimensional axisymmetric coordinates were used to establish the numerical model for the GMAW fume flow.A transient finite-volume method with non-staggered mesh was applied to solve the numerical model. The numerical simulations were run $2.0 \leq Pr \leq 15.0$ with other parameters kept constant at Fr = 5.5, Re = 100, and $H/X_0 = 10$. The time series of the spreading distance plotted at various Prnumbers show different types of distances at different stages of the fume flow, the initial maximum, the maximum, and the final distances. When the Pr number is increased from 2.0 to 15.0.the gap between the initial maximum and the maximum distances decreases while the gap between the initial maximum and the final distances decreases.A nonlinear relationship was observed when the initial maximum and final distance data were plotted against the Pr number. The best fit for the initial maximum and the final distance data were obtained using the power of -1/2 and -2/3

1. Introduction

Nowadays, Gas Metal Arc Welding (GMAW) is one of the most popular welding methods. It plays a vitalrole in modern manufacturing industries that account for more than 70% of welding processes in modern manufacturing industries with a wide range of applications in shipbuilding, pipeline, automotive, aerospace, defense, and construction[1]–[3]. As GMAW involves using shielding gas, the welding process produces a large amount of fume, which may spread to the surroundings, including the breathing zone of the welding operator. Gonser and Hogan [4]studied the health issues from arc welding fume exposure. They mentioned the hazardous elements that the GMAW might produce and discussed the acute and chronic diseases associated with those elements. Schoonover et al. [5] measured the exposure of welding fume metals of workers in a large manufacturing facility. They found that the welding operators were exposed to a significantly higher concentration of welding fume metals of 474 $\mu g/m^3$ compared to only 60 $\mu g/m^3$ for non-welders. When the number was further explored, they found that welders who performed GMAW were exposed to higher concentrations of welding fume metals than those who used Gas Tungsten Arc Welding (GTAW).

There have been many efforts to minimize the negative effect of the fume produced by GMAW on the welding operators by studying the jet flow behavior of the fume of the GMAW. Orakwe et al. [6]examined the jet flow characteristics coming out of the nozzle of GMAW at room temperature conditions. They combined the Particle Image Velocimetry (PIV) method for visualizing the jet flow with the Computational Fluid Dynamics (CFD) method by using a CFD package TASCflowfor further analysis. They found essential flow characteristics for optimizing weld pool protection by the shielding gas. Johnson et al. [7] further study the jet flow of the GMAW. They examined the shielding gas flow behavior at room temperature. They used a laser light sheet to illuminate smoke-seeded shielding gas to visualize the flow and PIV to measure the gas velocity. They were able to produce more reliable results for turbulent velocity measurements that were useful for characterizing the flow field of the nozzle and gas flow. Godbole et al. [8]studied the flow field of the GMAW process by combining numerical and experimental methods to optimize the design of a fume extraction system. They used a CFD package to conduct numerical simulations and applied physical modeling using a saline solution to validate the numerical model. They used Light-Induced Fluorescence (LIF) to visualize the physical model. They discovered the essential structures of the smoke of GMAW, which were utilized to develop a novel on-torch welding fume extraction system.

In this study, the model for investigating GMAW fumebehavioris developed from the theory of negative buoyancy jets, often called fountains. As there have been plenty of studies in this area, only a few are cited and considered when developing the model. Bloomfield and Kerr [9] studied turbulent fountains injected into a stably stratified ambient using a combination of both theoretical and numerical. Their numerical model was developed using a set of entrainment equations. They used the numerical solutions for their experimental setup, which was made from a dense salt solution injected upward into an acrylic tank, whereas the stratified environment was established using the double bucket method. They found that the downflow of the jet may spread at the base or at an intermediate height

Journal of Welding Technology
P-ISSN: 2716-1471 | E-ISSN: 2716-0475
http://e-jurnal.pnl.ac.id/Welding_Technology

depending on the strength of the stratification, the momentum fluxes,and the buoyancy at the source. In their following paper, Bloomfield and Kerr refined their theoretical model for fountains in both homogenous and stratified ambient [10]. They developed four different models, which consisted of two models for body force formulations and the rest were two formulations of the rate of entrainment between the jet flow. The accuracy of their models when validated with experimental data, was 15% for fountains in homogenous ambient and 5% for fountains in stratified ambient.

Later studies on negative jet flows focused more on numerical approaches especially using CFD simulations. Lin and Armfield [11]investigated two-dimensional axisymmetric weak fountains injected into a homogeneous environment numerically using direct simulation CFD by solving non-dimensional Navier-Stokes and energy equations. They studied the fountain flow at Froude number $0.1 \leq Fr \leq 1.0$, Reynolds number Re = 200, and Prandtl number, Pr= 7.0. Fr and Re in their study are defined as follows,

$$Fr = \frac{V_0}{\sqrt{X_0 \sigma_0}} \quad (1)$$

and

$$Re = \frac{V_0 X_0}{\nu} \quad (2)$$

where V_0 is the velocity of the jet at the source, X_0 is the radius of the jet, σ_0 is reduced gravity, and ν is the kinematic viscosity of the source fluid. While Pr number is defined as,

$$Pr = \frac{\nu}{\kappa} \quad (3)$$

where κ is the thermal conductivity of the jet fluid. They found that the fountain initial and final heights are a function of the Fr number only. Later in their other paper, Lin and Armfield found that the fountain heights also depend on Re and Pr[12], [13]. Lin and Armfield thenstudied fountain flow in stratified ambient, where they found that the strength of the ambient stratification also affects the fountain heights [14]. Williamson et al. continued their studies by conducting three-dimensional (3D) direct numerical simulations (DNS) of weak turbulent fountains [15]. Their simulations were performed at $0.1 \leq Fr \leq 2.1$, $20 \leq Re \leq 3494$, and $0.7 \leq Pr \leq 50$. They made a comprehensive summary of fountain studies and plotted them in a chart. They found that the fountain heights depend only on the Fr number. In their following paper, Williamson et al. [16] investigated strong turbulent fountains using the same method and numerical model applied in their previous study. They performed their numerical simulation at $4 \leq Fr \leq 7$ and Re = 3350. They revealed the detailed structure of the fountain at inner upflow and outer downflow. They still found that the fountain heights depended on only the Fr number.

The negative jet or fountain flows used for establishing the model for the fume of GMAW welding are the fountains that strike on a surface or are oftencalled impinging fountains. There have been quite a few studies done in this area, although not as many as turbulent fountains. Lemckert and his colleagues have done significant work on experimental impinging fountains [17]–[20]. Holstein and Lemckert[18] studied fountains impinging on a solid surface experimentally by injecting fresh water downward into an acrylic tank filled with a saltwater solution. They modified the turbulent fountain height into the total distance traveled before the impinging fountains start to detach from the floor and rise as,

$$\frac{H + X_d}{X_0} = C.Fr^n \quad (4)$$

where H is the depth of the domain measured from the source, X_d is the radius at which the fountains start to detach from the floor, and C and nare constant found from the experiments to be C =13 and n = 0.4. Later, Lemckert[20] investigated fountains impinging on a free surface experimentally using a saltwater solution. Unlike the previous work that injected freshwater downward, he pumped dense saltwater upward into an acrylic tank filled with fresh water. Using the same correlation in equation (4), they found C = 4.8 and n = 0.74.

Recent studies on impinging fountain flows have shifted toward numerical methods as the speed of desktop computers has become fast enough to perform CFD simulation with reasonably good accuracy. Srinarayana et al. [21] studied planar impinging fountains numerically using an open-source CFD package Gerris. Their numerical simulations were conducted at $8 \leq Fr \leq 20$, $50 \leq Re \leq 1000$, and $7 \leq Pr \leq 700$ with domain height varied at $10 \leq H/X_0 \leq 30$. They applied dimensional analysis to correlate the dimensionless spreading distance X_d with Fr, Re, Pr, and H/X_0 and validated the empirical correlation obtained using the numerical results. In their other paper, Srinarayana et al. [22] also investigated the effect of opposing heat flux at the impinging surface. They modified their dimensional analysis parameters by adding heat flux as an additional term. The heat flux was added to the final correlation obtained in dimensionless form as $\Delta\theta.X_0/H$, which was then validated using numerical simulation results. They still used the Gerris CFD package for performing the numerical simulations,although they changed the meshing strategy using adaptive mesh. Recently, Luthfi [23] investigated the influence of height on the spreading distance of 2D axisymmetric impinging fountains by performing CFD direct numerical simulations using a set of programming codes written in Fortran. The illustration of the typical impinging fountain flow investigated is shown in Fig. 1. He found that the spreading radius where the fountains detach from the surface is scaled to the domain height as $X_d \sim H^{-1/2}$.

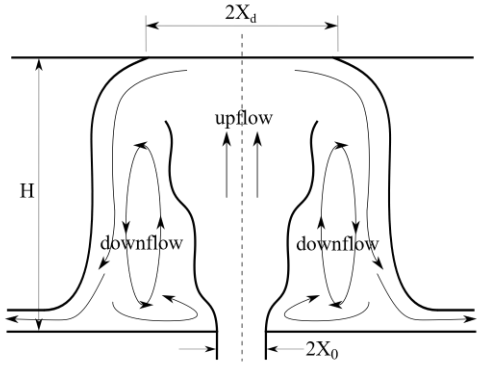

Fig. 1. Illustration of impinging fountain flow

Journal of Welding Technology
P-ISSN: 2716-1471 | E-ISSN: 2716-0475
http://e-jurnal.pnl.ac.id/Welding_Technology

As many studies of fountains found in the literature listed Pr number as one of the critical parameters that affect the behavior of the negative jets, in this study, the influence of the Pron the fume behavior of GMAW will be studied and explored. Based on the definition of Pr number as formulated in equation (3), it strongly depends on the composition of the fume. Apart from the welding particle contents as well as the smoke from high-temperature arc welding, the type of shielding gas used in GMAW contributes to the Pr number of the fume. Kumar et al. [24]made an effort to reduce the emission from GMAW by varying the compositionofthe shielding gas used in GMAW. They mixed CO_2 gas with pure argon and he tested different compositions of the mixture. They found lower emissions with the mixture that used lower CO_2 in the shielding gas. No information on the fume flow behavior was given, although it is strongly related to the emission level, especially in the breathing zone of the welding operator. Hence, this is the area of interest that will be investigated in this study.

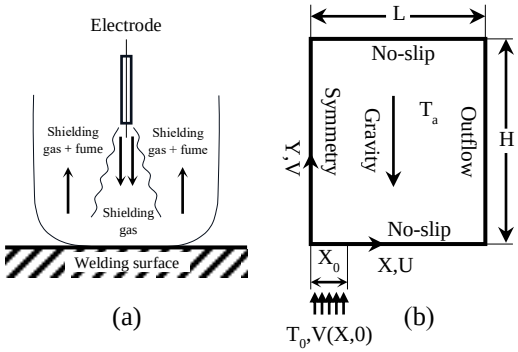

Fig. 2. The domain of physical system (a) Illustration GMAW fume flow and (b) numerical domain.

2. Research Methods/ Materials and Methods

The behavior of the fume of GMAW in this study was investigated numerically by solving a set of Navier-Stokes equations together with energy equations using programming codes written in Fortran, which were run in the Debian Linux operating system. The domain of the physical system of the fume flow is considered to be a cylinder in a vertical orientation having a Newtonian fluid at rest with a uniform temperature of T_a(Fig. 2). The top surface is set as a wall, and the side is an outflow where the flow exits the domain. The source fluid enters the domain from an orifice with a radius of X_0 located at the bottom center, while the rest of the bottom is set as a wall.

The Navier-Stokes equations for describing the flow are written in conservative and nondimensional in cylindrical coordinates. The energy equation includes the Boussinesq assumption for modeling the temperature distribution, density field in the domain, andfluid flow from the inlet. The modified equations for modeling the flow fume of GMAW investigated in this study are written as follows,

$$\frac{1}{x}\frac{\partial}{\partial x}(xu)+\frac{\partial v}{\partial y}=0 \tag{5}$$

$$\frac{\partial u}{\partial \tau}+\frac{1}{x}\frac{\partial}{\partial x}(xuu)+\frac{\partial}{\partial y}(uv)=-\frac{\partial p}{\partial x}+\frac{1}{Re}\left\{\frac{\partial}{\partial x}\left[\frac{1}{x}\frac{\partial}{\partial x}(xu)\right]+\frac{\partial^2 u}{\partial y^2}-\frac{u}{x^2}\right\} \tag{6}$$

$$\frac{\partial v}{\partial \tau}+\frac{1}{x}\frac{\partial}{\partial x}(xuv)+\frac{\partial}{\partial y}(vv)=-\frac{\partial p}{\partial y}+\left[\frac{1}{x}\frac{\partial}{\partial x}\left(x\frac{\partial v}{\partial x}\right)+\frac{\partial^2 v}{\partial y^2}\right]+\frac{1}{Fr^2\theta} \tag{7}$$

$$\frac{\partial \theta}{\partial \tau}+\frac{1}{x}\frac{\partial}{\partial x}(xu\theta)+\frac{\partial}{\partial y}(v\theta)=\frac{1}{RePr}\left[\frac{1}{x}\frac{\partial}{\partial x}\left(x\frac{\partial \theta}{\partial x}\right)+\frac{\partial^2 \theta}{\partial y^2}\right] \tag{8}$$

In these equations, all variables are non-dimensional where x and y are the dimensionless radial and axial distances, u and v are the dimensionless radial and axial velocities, p is the dimensionless pressure, τ is the dimensionless time, and θ is the dimensionless temperature. The non-dimensional quantities were calculated according to what Lin and Armfield [11] suggested in their paper,

$$x=\frac{X}{X_0}, y=\frac{Y}{X_0},\quad u=\frac{U}{V_0}, v=\frac{V}{V_0},\quad \tau=\frac{t}{(X_0/V_0)}, p=\frac{P}{\rho V_0^2}, \theta=\frac{T-T_a}{T_0-T_a} \tag{9}$$

where t is time in s, P is pressure in Pa, ρ is density in kg/m^3, and T is temperature in K. The initial conditions required for running the simulation are

$$u=0, v=0, \text{and} \theta=0 \quad \text{for all } x \text{ and } y \text{ with } \tau<0 \tag{10}$$

All the equations involved in the numerical model were discretized and solved in finite volume on a non-staggered cartesian mesh. A second-order central scheme with an ULTRA flux limiter was chosen for discretising the spatial part of the equations, while a second-order Adams-Bashford forward-in-time scheme was applied for the advection parts. For the viscous terms, the discretization was done using the Crank-Nicholson method, and the fractional step pressure correction method was applied to induce divergent free conditions and to renew the value of the pressure field. The velocity on the cell face in the pressure solver was obtained by momentum interpolation using the Rhie-Chow method. The discretization of the governing equations on the specified mesh resulted in a set of linear equations with central coefficient dominant that were solved using the BI-CSTAB method with a Jacobi preconditioned multigrid.

For running the numerical simulation, the length and the height of the domain, as shown in Fig. 2, were set to L = $7X_0$ and H = $10X_0$, respectively. The mesh size in the y direction was set uniform and very small, while in the x direction, the mesh was set finer around the orifice and gradually increased in size as it got closer to the outflow. This grid configuration resulted in a total of 623 × 243 cells. Most main parameters were set constant at Fr = 5.5 and Re = 100 except the investigated parameter, Pr number, which was varied from Pr = 2.0 up to Pr = 15.

Journal of Welding Technology
P-ISSN: 2716-1471 | E-ISSN: 2716-0475
http://e-jurnal.pnl.ac.id/Welding_Technology

3. Results and Discussion.

The time series of the spreading distance of the fume,as plotted in Fig. 3 shows that the Pr number does have a considerable effect on the spreading distance. It is obvious thatthe fumes flow at a lower Pr number have a higher spreading distance from the beginning when the flows start detaching from the surface until they reach a quasi-equilibrium state. In addition to that, the way the spreading distances reach the maximum value is also affected to some extent. In general, the spreading distance reaches the maximum in two steps. The flow initially peaks at a distance called an initial maximum distance, and then it stabilizes for a while before reaching the maximum distance. For fumePr = 2.0, the spreading distance decreases after reaching the initial maximum, and the difference between the initial maximum and the maximum value is subtle. This is in contrast with fume at Pr = 15.0, where the flow of fume does not decrease after reaching the initial maximum, and it further increases to the maximum value, which is noticeably higher than the initial maximum value.

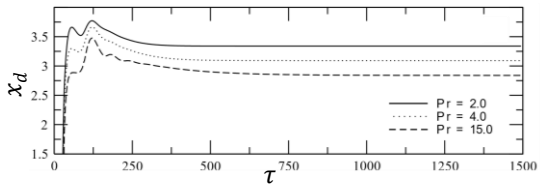

Fig. 3. The spreading distance, x_d plotted over time at various Pr numbers.

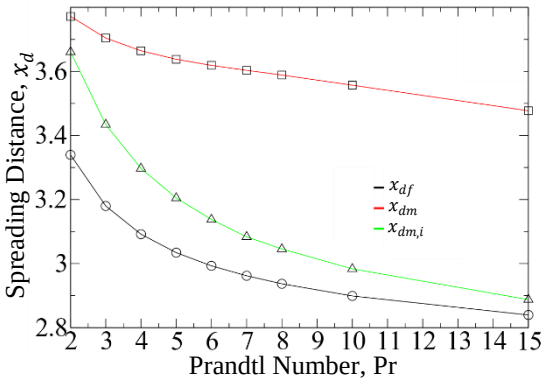

Fig. 4. The spreading distance at different stages, initial maximum, maximum, and final spreading distance plotted against Pr number.

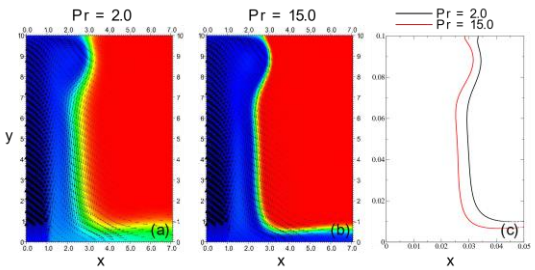

Fig. 5. The comparison of the temperature contour of the jets obtained at (a) Pr = 2.0 and (b) Pr = 15.0. (c) Iso profile temperature.

To validate the statement about the gap between the initial maximum $x_{dm,i}$, the maximum x_{dm}, dan the final spreading radius x_{df}, those values were extracted from the time series plot in Fig. 3 and plotted separately as a function of Pr number in Fig. 4. The trend of $x_{dm,i}$, x_{dm}, and x_{df} confirms that the change of the gap between the spreading radius at different stages of flow development of fume spreading distance does exist. It is obvious that the gap between the spreading distance $x_{dm,i}$ (green line) and x_{dm} (red line) at Pr =2.0 is narrow, and it grows significantly as the Pr is increased to 15.0. However, there is an interesting part that was not clearly seen in Fig. 3. The gap between the initial maximum $x_{dm,i}$ (green line) and final distance x_{df} (black line) decreases when the Pr number is increased from 2.0 to 15.0.

The plot of temperature contour and iso profile temperature at the minimum Pr = 2.0 and the maximum Pr = 15.0, as shown in Fig. 5 reveals the reasons why the spreading distance changes when the Pr number is increased. The blue part of the image in Fig.s 5(a) and 5(b) is the fume fluid while the red part is the ambient fluid. The boundary between both parts is the boundary layer where the mixing between fume fluid and ambient fluid occurs. This part is where the differences between both fumes are noticeable. The flow at Pr = 2.0 is highly diffuse with a thicker boundary layer between the fume flow and the ambient fluid than at Pr = 15.0. The differences in boundary layer thickness are the main cause of why the spreading distance at a low Pr number is larger than at a high Pr number. The iso temperature profile of both flows, as plotted in Fig. 5(c), shows that not only the spreading radius but the overall thickness of the jet at Pr = 2.0 are larger.

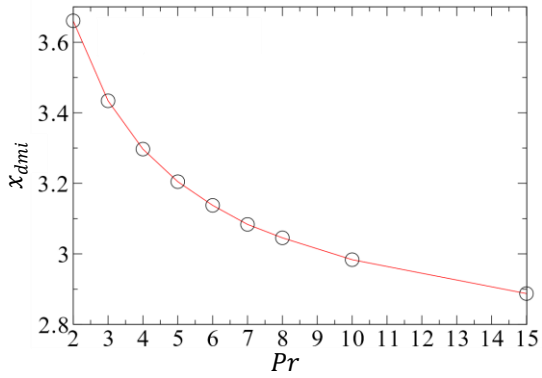

Fig. 6. The raw data of the initial maximum spreading distance, $x_{dm,i}$ plotted against the Pr number.

The raw data of the initial maximum spreading distance plotted against the Pr number,as presented in Fig. 6, shows a typical nonlinear relationship. Lin and Armfield [12] suggest a power relation Pr^c between the thickness of the boundary layer and Pr number with c = -1/2. Careful testing by trial and error found that the best power with the lowest fitting error was found at c = -1/2, the same as what Lin and Armfield suggested in their paper[12], [13], [25]. By updating the axis into $Pr^{-1/2}$, as done in Fig. 7, a highly accurate linear regression line can fit the data very well with an accuracy of R^2 = 0.9998884. The resulting equation from the linear regression curve fitting is,

$$x_{dm,i} = 2.4349 + 1.7286Pr^{-\frac{1}{2}} \qquad (11)$$

Journal of Welding Technology
P-ISSN: 2716-1471 | E-ISSN: 2716-0475
http://e-jurnal.pnl.ac.id/Welding_Technology

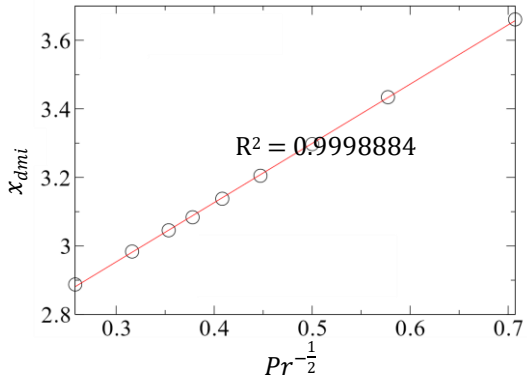

Fig. 7. The initial maximum spreading distance, $x_{dm,i}$ plotted against the scaled Pr number.

As the maximum spreading distance data may change inconsistently within the Pr number range investigated in this study, the trend of the data is difficult to find.When this paper is written, the correlation has not yet been successfully established. Fortunately, the data for the final spreading distance are easier to analyze. The raw data of the final spreading distance when the jet has reached quasi-equilibrium, as shown in Fig. 8, create a similar nonlinear trend to the previous graph when plotted against the Pr number,although the power required for producing the best fitting curve with the lowest error possible is not exactly the same. By performing careful searching by trial and error, it was found that the best fit can be obtained by using $Pr^{-3/2}$. When updating the x-axis into $Pr^{-2/3}$, the data for the final spreading distance produce a linear trend that can be well fitted using a linear regression line witha very high accuracy of R^2 = 0.999151 (Fig. 9). The equation obtained from fitting the data with a linear regression line is,

$$x_{df} = 2.6689 + 1.0655Pr^{-\frac{2}{3}} \quad (12)$$

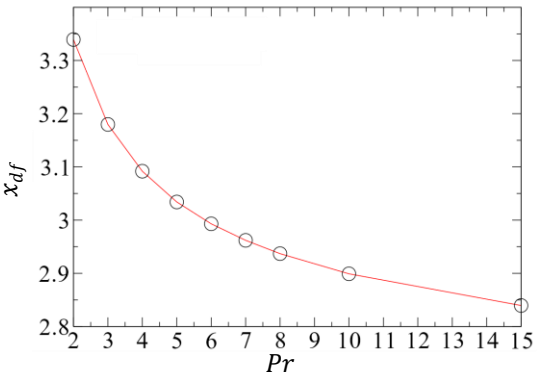

Fig. 8. The raw data of the final spreading distance, x_{df} plotted against the Pr number.

The results obtained in this study imply that the behavior of welding fumes at different Pr numbers used should be considered when using GMAW for welding as the fume may harmfully flow to the breathing zone of the welding operator. Pr number of the fume flow may changewhen the welding surface becomes hotter or when more metal particlesare trapped into the fume changing the properties of the fume.

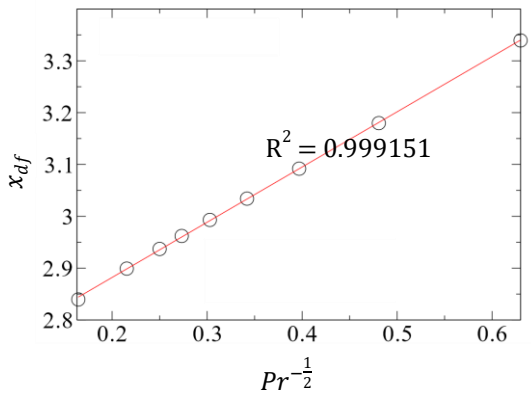

Fig. 9. The final spreading distance, x_{df} plotted against the scaled Pr number.

4. Conclusions.

The effect of the Pr number on the behavior of the fume of GMAW has been investigated numerically using the CFD method. The time series of the spreading distance where the flow starts detaching from the surface has been obtained at various Pr numbers, and three different types of distances have been identified, the initial maximum, the maximum, and the final spreading distances. The gap between the initial maximum and the maximum distances increasesconsiderably at a larger Pr number. On the contrary, the gap between the initial maximum and the final distances slightly decreases when the Prandtl number of the flow is increased. The flows of the jet at a lower Pr number have larger spreading distances due to a thicker boundary layer between the jet flow and the ambient fluid. A nonlinear relationship was observed when the data for the initial maximum and the final distance were plotted against the Pr number. The initial maximum distance can be fitted well using a linear regression fitting curve when a power of -1/2 was applied to the data,while the data for the final distance can be fitted using a power of -2/3.

References.

[1] P. Kah, *Advancements in Intelligent Gas Metal Arc Welding Systems: Fundamentals and Applications*. Elsevier, 2021.

[2] J. Juwanda, S. Saifuddin, and M. Marzuki, "Analisa pengaruh kuat arus hasil pengelasan GMAW terhadap kekerasan material ASTM A 36," *J. Weld. Technol.*, vol. 3, no. 1, pp. 6–11, 2021.

[3] Z. Özdemir, "Effect of Shallow Cryogenıc Heat Treatment on Metal Inert Gas Weldıng Zone of S 355 J2 Steel," *J. Weld. Technol.*, vol. 5, no. 1, pp. 1–5, 2023.

[4] M. Gonser and T. Hogan, "Arc welding health effects, fume formation mechanisms, and characterization methods," *Arc Weld.*, pp. 299–320, 2011.

[5] T. Schoonover, L. Conroy, S. Lacey, and J. Plavka, "Personal exposure to metal fume, NO2, and O3 among production welders and non-welders," *Ind. Health*, vol. 49, no. 1, pp. 63–72, 2011.

[6] P. A. Orakwe, D. A. Johnson, and E. J. Weckman, "Examination of welding nozzle Jet flow at cold flow conditions," in *Fluids Engineering Division Summer Meeting*, 2002, vol. 36169, pp. 3–11.

[7] D. A. Johnson, P. Orakwe, and E. Weckman,

"Experimental examination of welding nozzle jet flow at cold flow conditions," *Sci. Technol. Weld. Join.*, vol. 11, no. 6, pp. 681–687, 2006, doi: 10.1179/174329306X148200.

[8] A. Godbole, P. Cooper, and J. Norrish, "Design and optimization of a novel on-torch fume extraction device using CFD and fluid simulation," *Weld. World*, vol. 54, pp. R80–R86, 2010.

[9] L. J. Bloomfield and R. C. Kerr, "Turbulent fountains in a stratified fluid," *J. Fluid Mech.*, vol. 358, pp. 335–356, 1998, doi: 10.1017/S0022112097008252.

[10] L. J. Bloomfield and R. C. Kerr, "A theoretical model of a turbulent fountain," *J. Fluid Mech.*, vol. 424, pp. 197–216, 2000, doi: 10.1017/S0022112000001907.

[11] W. Lin and S. W. Armfield, "Direct simulation of weak axisymmetric fountains in a homogeneous fluid," *J. Fluid Mech.*, vol. 403, pp. 67–88, 2000, doi: 10.1017/S0022112099006953.

[12] W. Lin and S. W. Armfield, "The Reynolds and Prandtl number dependence of weak fountains," *Comput. Mech.*, vol. 31, no. 5, pp. 379–389, 2003, doi: 10.1007/s00466-003-0440-5.

[13] W. Lin and S. W. Armfield, "Onset of entrainment in transitional round fountains," *Int. J. Heat Mass Transf.*, vol. 51, no. 21–22, pp. 5226–5237, 2008, doi: 10.1016/j.ijheatmasstransfer.2008.02.047.

[14] W. Lin and S. W. Armfield, "Weak fountains in a stratified fluid," *Phys. Rev. E - Stat. Physics, Plasmas, Fluids, Relat. Interdiscip. Top.*, vol. 66, no. 6, p. 10, 2002, doi: 10.1103/PhysRevE.66.066308.

[15] N. Williamson, S. W. Armfield, and W. Lin, "Transition behaviour of weak turbulent fountains," *J. Fluid Mech.*, vol. 655, pp. 306–326, 2010, doi: 10.1017/S002211201000087X.

[16] N. Williamson, S. W. Armfield, and W. Lin, "Forced turbulent fountain flow behaviour," *J. Fluid Mech.*, vol. 671, pp. 535–558, 2011, doi: 10.1017/S0022112010005872.

[17] K. Kuruppu and C. J. Lemckert, "Plunging radius of water fountains following impact on a rigid surface," in *7th Australasian Heat and Mass Transfer Conference, Townsville, Queensland, Australia*, 2000, pp. 195–200.

[18] D. M. Holstein and C. J. Lemckert, "Spreading of energetic submerged fountains impinging on a rigid surface," in *14th Australasian Fluid Mechanics Conference, Adelaide University, Adelaide, Australia*, 2001, pp. 10–14.

[19] C. J. Lemckert, "Submerged fountains impinging on a smooth horizontal surface," 2005.

[20] C. J. Lemckert, "Spreading radius of fountains after impinging a free surface," in *Proceedings of the 15th Australasian Fluid Mechanics Conference*, 2004, vol. 400, pp. 217–220.

[21] N. Srinarayana, S. W. Armfield, and W. X. Lin, "Impinging plane fountains in a homogeneous fluid," *Int. J. Heat Mass Transf.*, vol. 52, no. 11–12, pp. 2614–2623, 2009, doi: 10.1016/j.ijheatmasstransfer.2009.01.009.

[22] N. Srinarayana, S. W. Armfield, and W. Lin, "Laminar plane fountains impinging on a ceiling with an opposing heat flux," *Int. J. Heat Mass Transf.*, vol. 52, no. 19–20, pp. 4545–4552, 2009, doi: 10.1016/j.ijheatmasstransfer.2009.03.015.

[23] Luthfi, "The influence of height on the spreading distance of axisymmetric jets impinging on a rigid surface," *J. Polimesin*, vol. 20, no. 1, pp. 18–23, 2022.

[24] K. V. Satheesh Kumar, P. Selvak umar, K. R. Uvanshankar, S. Thirunavukarasu, V. Vijay Anand, and D. Vishal, "Investigation on the effect of technological parameters on emission factor in 316l stainless steel using gas metal arc welding," *Arch. Metall. Mater.*, vol. 66, no. 2, pp. 609–615, 2021, doi: 10.24425/amm.2021.135898.

[25] W. Lin and S. W. Armfield, "Direct simulation of fountains with intermediate Froude and Reynolds numbers," *ANZIAM J.*, vol. 45, p. 66, 2004, doi: 10.21914/anziamj.v45i0.873.